NUSAP1 promotes gastric cancer radioresistance by inhibiting ubiquitination of ANXA2 and is suppressed by miR-129-5p

Yugang Ge[1] · Biao Wang[2] · Jian Xiao[3] · Hongshuai Wu[4] · Qing Shao[1]

Abstract

Background Radiotherapy is an important strategy for the treatment of advanced gastric cancer (GC), while the radioresistance limits its effectiveness. Nucleolar and spindle associated protein 1 (NUSAP1) was implicated in cancer progression and chemoresistance. However, the underlying mechanisms of NUSAP1 influencing GC radioresistance remain largely unknown.

Methods Meta-analysis was conducted to systematically evaluate the prognostic value of NUSAP1 in human cancers. Gene set enrichment analysis (GSEA) was conducted using The Cancer Genome Atlas (TCGA) and gene expression omnibus (GEO) datasets. MRNA and protein expressions were detected by qRT-PCR and western blot, respectively. The radiosensitivity of GC cells was observed by colony formation, flow cytometry, comet, immunofluorescence, and animal assays. Immunoprecipitation assay and mass spectrometry were utilized to identify protein associations. MiRNAs binding with NUSAP1 were determined by starbase prediction, luciferase reporter, and RNA immunoprecipitation (RIP) assays.

Results NUSAP1 high expression predicted worse overall survival (OS) and disease-free survival (DFS) with no statistical heterogeneity through the meta-analysis. Downregulation of NUSAP1 significantly increased GC radiosensitivity by inhibiting colony formation, DNA damage repair, and promoting apoptosis following irradiation. Additionally, NUSAP1 silencing combined with radiation resulted in a synergistic anti-tumor effect in xenograft mouse model. Mechanistically, NUSAP1 interacted with ANXA2, protecting it against protein degradation via impeding its ubiquitination process. NUSAP1 was confirmed as a target of miR-129-5p and negatively regulated by it.

Conclusion Our results suggested that NUSAP1 enhanced the radioresistance of GC cells. NUSAP1 could be a promising target to increase GC radiosensitivity.

Keywords NUSAP1 · Gastric cancer · Radioresistance · ANXA2

Yugang Ge, Biao Wang and Jian Xiao contributed equally to this study.

✉ Qing Shao
jyqingshao@sina.com

1 Department of General Surgery, Jiangyin People's Hospital, The Affiliated Jiangyin Clinical College of Xuzhou Medical University, Jiangyin, Jiangsu Province, China

2 Department of Oncology, First People's Hospital of Yancheng, Fourth Affiliated Hospital of Nantong University, Yancheng, China

3 Department of General Surgery, The First Affiliated Hospital of Nanjing Medical University, Nanjing, Jiangsu Province, China

4 Wuxi Key Laboratory of Biomaterials for Clinical Application, Department of Central Laboratory, Jiangyin Clinical College of Xuzhou Medical University, Wuxi, China

Introduction

Gastric cancer (GC) ranks fifth in the incidence of all malignant tumors and third in cancer-related deaths around the world (Smyth et al. 2020). With the increasing understanding of its pathogenesis, multiple strategies have been used in the diagnosis and treatment of GC, including surgical resection, chemotherapy, radiotherapy, and molecular targeted therapy (Sexton, Al Hallak, Diab, & Azmi, 2020). The five-year survival rate of early-stage GC patients undergoing surgery can reach 90 to 100%, even so, patients suffering from advanced GC possess a five-year survival rate of less than 30% (Song et al. 2017). In recent years, with the rapid development of radiotherapy equipment and technology, more and more attention has been paid to the role of radiotherapy in the comprehensive treatment of GC. Various

studies have shown that radiotherapy can effectively reduce the local recurrence rate of GC after surgery and improve the prognosis of partial patients (Park et al. 2015; Yu et al. 2018). There are many organs around the stomach and gastric adenocarcinoma is known as not sensitive to radiotherapy. High dose of gastric irradiation will inevitably bring about obvious toxic reactions, including gastric ulcer, normal gastric tissue fibrosis, intestinal perforation, radioactive liver injury, and pancreatic injury. Hence, it is necessary to explore potential radiosensitizers to improve the effectiveness of radiotherapy.

Nucleolar and spindle associated protein 1 (NUSAP1), as a microtubule-associated protein, participated in chromosome separation, cytokinesis, spindle assembly, and ubiquitin-dependent proteolysis (Li et al. 2016; Raemaekers et al. 2003). Besides, NUSAP1 played a vital role in cancer biology. Previous researches revealed that NUSAP1 was abnormally expressed in a variety of tumors. In pancreatic ductal adenocarcinoma, NUSAP1 bound with transcription factor c-Myc and HIF-1α to form a complex, increasing LDHA expression and promoting warburg effect and metastasis (Chen et al. 2023). NUSAP1 enhanced cancer stemness via interacting with RACK1 to stimulate STAT3 nuclear translocation in hepatocellular carcinoma (Li et al. 2022). NUSAP1 could facilitate chemoresistance by inhibiting the ubiquitination of ATR to potentiate DNA damage repair (Zhao et al. 2020). Meanwhile, numerous signaling pathways were modulated by NUSAP1, including Hedgehog (Winkelmann et al. 1986), PI3K/AKT (Luo et al. 2022), AMPK/PPARγ (Qiu et al. 2021), Wnt/β-catenin (Zhang et al. 2020), and so on. NUSAP1 high expression was also confirmed to be closely correlated with poor prognosis of cancer patients , such as ovarian cancer (Gou et al. 2022) , non-small cell lung cancer (Ling et al. 2021), and bladder cancer (Chen et al. 2021). Our previously published article showed that downregulation of NUSAP1 attenuated cell proliferation, migration, and invasion through suppressing mTORC1 signaling pathway in GC (Ge et al. 2020). However, the role and mechanism of NUSAP1 in radioresistance of GC have not been clarified yet.

In this report, we firstly gathered all eligible articles to evaluate the prognostic and clinicopathological value of NUSAP1 in human malignancies by conducting a meta-analysis. Gene set enrichment analyses (GSEA) were performed using the data from The Cancer Genome Atlas (TCGA) and gene expression omnibus (GEO) database, gaining functional insights into the mechanisms of radioresistance. Then a series of functional assays were carried out to investigate the influence of NUSAP1 on GC radiosensitivity in vitro and in vivo. Finally, we explored the relevant molecular mechanisms of NUSAP1 inducing GC radioresistance.

Materials and methods

Search strategy and study selection

Up to August 11, 2024, potential eligible literatures which analyzed the association between NUSAP1 and the prognosis or clinicopathologic features of cancer subjects were searched in the following databases: PubMed, Web of Science, Embase, Ovid, and Cochrane Library. The following keywords for searching: ("NUSAP1" or "nucleolar spindle-associated protein 1") and ("cancer" or "carcinoma" or "tumor" or "malignancy" or "neoplasm") were used. We also obtained the additional articles through screening the reference lists of above retrieved publications.

Eligible studies met these criteria: (a) NUSAP1 expression in cancer specimens was detected, and patients were grouped according to its expression levels; (b) articles assessing the correlation of NUSAP1 with the prognostic and clinicopathologic features of cancer patients; (c) sufficient data for calculating the hazard ratio (HR) with 95% confidence interval (CI) for overall survival (OS) and disease-free survival (DFS). The exclusion criteria were as follows: (a) reviews, case reports, letters, comments, and abstracts; (b) studies only exploring the functions and molecular mechanism of NUSAP1, or bioinformatics articles; (c) researches where the required data could not be extracted.

Data extraction and quality assessment

All the essential data from each identified publication were extracted by two investigators (Yugang Ge and Biao Wang) independently, including first author's name, publication year, cancer resource, tumor type, total cases, the number of patients in high and low NUSAP1 expression groups, method of NUSAP1 detecting, outcome measures, survival analysis method, follow-up period, HRs and the corresponding 95% CIs of OS and DFS, as well as patient number for TNM stage, lymph node metastasis, distant metastasis, differentiation, and tumor size. If HRs and 95% CIs were evaluated via univariate and multivariate analysis, the latter was the priority. Engauge Digitizer Version 4.1 (Tierney et al. 2007) was used to extract the survival data from Kaplan–Meier curves when these data were not available. We conducted the quality assessment in line with Reporting Recommendations for Tumor Marker Prognostic Studies (REMARK) guidelines (Supplementary Table 1). The researches with more than 60% scores were considered as high quality (Supplementary Table 2).

RNA isolation and qRT-PCR

Total RNA of cells was extracted using TRIzol reagent (Invitrogen, USA) according to the manufacturer's instructions. NanoDrop ND-2000 spectrophotometer (Thermo Fisher, USA) was applied to detect the concentration and quality of purified RNA. The reverse transcription was carried out employing HiScript III All-in-one RT SuperMix (Vazyme, R333-01). AceQ SYBR Green Master Mix (Vazyme, Q141-02) was adopted to perform the real-time qRT-PCR analyses. GAPDH was used as the internal standard. The Revert Aid First Strand cDNA Synthesis Kit (Thermo Scientific, USA) was adopted to reverse transcribe miRNAs following polyadenylation. MiRNA expression levels were normalized with U6. We utilized the $2^{(-\Delta\Delta CT)}$ method to calculated the relative expression. All the sequences of primers were listed in Supplementary Table 3.

Cell culture, transfection, and plasmid construction

The human GC cell lines MKN-45 and HGC-27 were purchased from Shanghai Institutes for Biological Sciences. Cells were cultured in RPMI 1640 medium (WISENT, Canada) supplemented with 1% penicillin/streptomycin (Gibco, USA) and 10% fetal bovine serum (Invitrogen, USA). All cell lines were incubated under standard conditions (37 °C, 5% CO_2). To establish stable NUSAP1/ANXA2-knockdown and NUSAP1/ANXA2-overexpression GC cells, short-hairpin RNA (shRNA) sequences were packaged in lentivirus vectors, NUSAP1/ANXA2 was cloned into pcDNA3.1 vector (GenePharma, China). MiRNA mimics and their negative controls were also designed and synthesized by GenePharma. Lipofectamine 3000 (Thermo Fisher, USA) was used to perform the transfection. The specific sequences were listed in Supplementary Table 4.

Dual luciferase reporter assay

The 3′-UTR sequences of NUSAP1 containing wild-type or mutated miR-129-5p binding sites were synthesized and inserted into the pGL3-basic luciferase reporter vector (Promega, USA). Using Lipofectamine 3000, the luciferase reporter vectors and miRNA mimics or control were co-transfected into HEK293T cells. We used the dual luciferase reporting system (Promega, USA) to measure the Firefly and Renilla luciferase activities 48 h post-transfection.

RNA immunoprecipitation (RIP)

The Magna RIP KIT (Millipore, USA) was applied to conduct the RNA immunoprecipitation assay according to the manufacturer's instruction. Briefly, cells were collected through centrifugation and lysed by NP40. Subsequently, cells were incubated with anti-Ago2 antibody coated magnetic beads at 4 °C overnight. The rabbit IgG antibody was used as a negative control. After proteinase K treatment, the coprecipitated RNAs were then detected by qRT-PCR.

Western blot and immunoprecipitation

RIPA buffer (Beyotime, China) was used to extract the total protein. Protein concentrations were determined by the BCA protein assay kit (Thermo Fisher, USA). Protein was separated through sodium dodecyl sulfate (SDS)–PAGE, followed by electrotransfer onto polyvinylidene difluoride (PVDF) membranes. Next, the membranes were incubated with indicated primary antibodies at 4 °C overnight after blocked with 5% BSA, followed the incubation by HRP-conjugated secondary antibodies for two hours at room temperature. Immunoreactive bands were visualized by ECL chemiluminescent reagents (Millipore, USA) via a Bio-Spectrum 600 Imaging System (Thermo Fisher, USA). The antibodies information was listed in Supplementary Table 5.

For immunoprecipitation (IP), we firstly mixed 500–1000 µg cell lysates and specified antibodies and incubated them overnight at 4 °C. Afterwards, above immune complex was mixed with protein A/G magnetic beads (Vazyme, China) and incubated for 0.5 h at room temperature. IP buffer was used to wash the magnetic beads twice, then pure water was applied to wash the antigen/antibody complex once. After added 1 × SDS loading buffer, the products were boiled for five minutes at 95 °C. The immunoprecipitated protein was analyzed through western blot or mass spectrometry (Thermo Fisher, USA).

Immunofluorescent staining

4% paraformaldehyde was used to fix the cells for 10 min. Then we added 1% Triton X-100 to improve membrane permeability for 10 min. Next, 5% BSA was added to block the non-specific binding for one hour. Above cells were incubated with the primary antibody against γH2AX at 4 °C overnight. After washed by PBS, the cells were incubated with the secondary antibody: Cy3-labeled goat anti–rabbit IgG for one hour at room temperature. Subsequently, nuclei were stained by DAPI. Finally, the images were captured via a laser confocal microscope (THUNDER DMi8, LEICA, German) to measure the fluorescence of γH2AX.

Comet assay

A CometAssay kit (Trevigen, USA) was used to conduct the neutral comet assay. Cells treated by 4 Gy irradiation were digested and resuspended in PBS at a density of 5×10^5

cells/ml. The cells were mixed with low-melting-point agarose gel and poured onto the slides. Dipping the slides in 4 °C lysis solution for 1 h increased the sensitivity. After washed by the neutral electrophoresis buffer for 30 min, the slides were subjected to electrophoresis at 21 V for 45 min. Next, the samples were placed in DNA precipitation solution for 0.5 h, followed in 70% ethanol for 0.5 h at room temperature. SYBR green I was adopted to stain the slides. CASP 1.2.3 beta 1 software (Krzysztof Konca, Poland) was used to analyze the percentage of DNA in the tail.

Clonogenic survival assay

Harvested GC cells were seeded into six-well plates at different densities: 300, 500, 1000, 2000, 4000 cells per well for 24 h. Then cells were subjected to doses of 0, 2, 4, 6, 8 Gy X-ray irradiation via a medical linear accelerator (Elekta, Sweden), respectively. After 2 weeks, 1% crystal violet was applied to stain the cells and the colonies containing ≥ 50 cells were counted. The plating efficiency equaled to the colonies counted/cells plated number of control group. Surviving fraction (SF) was calculated using the following formula: the number of colonies formed/(the total number of cells seeded $\times$ the plating efficiency). The survival curves were derived by the single-hit multiple-target model: $SF = 1 - (1 - EXP(-D/D0))^N$.

Flow cytometry analysis

The Apoptosis Detection Kit (Multisciences, China) was used to detect the apoptosis ratio of treated cells. The cells were harvested and resuspended by the binding buffer. Next, we added 5 µl Annexin-V-APC and 10 µl propidium iodide (PI) into the cell suspension and incubated them in the dark for five minutes. A flow cytometer (BD Biosciences, USA) was used to analyze the data.

Protein stability and degradation assay

In order to identify the half-life of ANXA2, we used a protein synthesis inhibitor cycloheximide (CHX) (100 µg/ml) to treat the cells in different groups for the indicated durations. Then the cells were harvested at different time points for western blotting. For the degradation assay, 10µM MG132 (Beyotime, China) was added to incubate the cells. After 24 h, we extracted the total protein to conduct western blot analyses.

Ubiquitination assay

GC cells were transfected with HA-Ub plasmid for 2 days, then treated by 10µM MG132 for 6 h before harvest. Cell lysates were incubated using the anti-ANXA2 antibody for co-immunoprecipitation, then the ubiquitination level of ANXA2 was evaluated by immunoblotting with an anti-HA antibody.

Animal experiments

We purchased 4-week-old female BALB/C nude mice from the Animal Experimental Center of Nanjing Medical University. Nude mice were randomly divided into four groups: (a) shNC, (b) shNUSAP1, (c) shNC+ionizing radiation (IR), and (d)shNUSAP1+IR. 4×10^6 cells were injected subcutaneously into the right groin of mice. The vernier caliper was applied to measure the size of tumors every three days. The tumor volumes were calculated through the following formula: $V(mm^3) = length \times width^2 / 2$. Mice were subjected to X-ray dosage of 8 Gy when the tumors had reached a volume of 200 mm³. 15 days later, tumor samples were collected and weighed. The entire experimental protocol was performed in accordance with the guidelines of the Animal Ethics Committee of Nanjing Medical University.

Immunohistochemistry staining (IHC)

The subcutaneous tumor specimens from nude mice were fixed by 4% paraformaldehyde, and cut into 4 µm-thick sections after embedded by paraffin. The tissue slides were deparaffinized with xylenes and rehydrated by graded ethanol washes, then treated by 3% hydrogen peroxide for 20 min to block endogenous peroxidase activity. The slides were incubated with specific primary antibodies overnight at 4 °C. After washing three times, sections were incubated with the corresponding secondary antibodies for 1 h at 37 °C. Finally, the sections were stained with diaminobenzidine solution and hematoxylin, which were then observed and photographed on a microscope. The antibody used was listed in Supplementary Table 5.

Statistical analysis and bioinformatics analysis

The SPSS25 and GraphPad Prism 6 were utilized to perform the statistical analyses, Stata MP14.0 was used for the meta-analysis. The prognostic value of NUSAP1 on OS/DFS and the correlation of NUSAP1 with clinicopathological characteristics in human cancers were estimated by pooled HRs with 95%CIs and pooled ORs with 95% CIs, respectively. The chi-squared Q test and I^2 statistics were applied to calculate the heterogeneity. When there was no obvious heterogeneity ($I^2 < 50\%$ or $P > 0.1$), the fixed effects model was chosen; otherwise, the random effects model was selected. We adopted Begg's funnel plots to determine the publication bias ($Pr > |z| \leq 0.1$ was considered as positive) and performed

sensitivity analyses to evaluate the stability of the results. The statistical difference between two groups was analyzed by Student's t-test, and the differences among multiple groups were assessed by analysis of variance. The TIMER (https://cistrome.shinyapps.io/timer/), GEPIA (http://gepia.cancer-pku.cn/), GEO (https://www.ncbi.nlm.nih.gov/gds/), and kmplot (https://kmplot.com/analysis/) databases were applied to analyze the expression of NUSAP1/ANXA2 in cancer or the association of them with patients prognosis. The UCSC cancer browser (https://xenabrowser.net/data-pages/) was used to evaluate miR-129-5p expression in GC. Data were shown as means ± standard deviation (SD). P values less than 0.05 were considered as statistically significant. GSEA was performed to determine the potential biological pathways between high-NUSAP1/ANXA2 and low-NUSAP1/ANXA2 groups. P values of the normalized enrichment score (NES) < 0.05 and false discovery rate (FDR) q values < 0.25 were considered as statistically significant. *$P < 0.05$, **$P < 0.01$, ***$P < 0.001$.

Results

## Included studies and characteristics in meta-analyses

As shown in Supplementary Figs. 1, 769 literatures were collected from the electronic databases, and then 451 articles were removed for duplications. Through screening the titles and abstracts carefully, 296 articles were eliminated, including reviews, letters, comments, abstracts, only cell or animal assays, bioinformatics articles, and studies not about NUSAP1. Regarding the rest 22 literatures, 9 studies lacking in the sufficient data were abandoned via reading the full texts. At last, 13 eligible articles were enrolled in the current meta-analysis. All studies were written by English, coming from China, Germany, and Egypt between 2015 and 2024. The sample size ranged from 46 to 248, among a total 1695 patients. 11 types of solid cancers were recorded including breast cancer (Chen et al. 2015) ($n = 1$), renal cell carcinoma (El-Hussieny et al. 2024; Fang et al. 2016) ($n = 2$), astrocytoma (Wu et al. 2017) ($n = 1$), colon cancer (Liu et al. 2018) ($n = 1$), hepatocellular carcinoma (Roy et al. 2018; Wang et al. 2019) ($n = 2$), esophageal squamous cell carcinoma (Guan et al. 2019) ($n = 1$), GC (Guo et al. 2020) ($n = 1$), bladder cancer (Chen et al. 2021) ($n = 1$), non-small cell lung cancer (Ling et al. 2021) ($n = 1$), ovarian cancer (Gou et al. 2022) ($n = 1$), pancreatic ductal adenocarcinoma (Liu et al. 2024) ($n = 1$). Briefly, qRT-PCR and IHC were adopted to measure NUSAP1 expression and the patients were split into two groups (low and high expression of NUSAP1). Multivariate analyses for OS were used in 5

studies. The details of included articles were summarized in Supplementary Table 6.

Association of NUSAP1 expression with survival and clinicopathological parameters

Via TIMER database analysis, it was found that NUSAP1 was highly expressed in vast majority of malignancies (Fig. 1A). Ten studies investigated the correlation between NUSAP1 expression and OS with a total of 1300 patients, and two studies explored the relationship between NUSAP1 expression and DFS with a total of 348 cases. We used the fixed effects model to estimate the pooled HR and 95%CI because no significant heterogeneity existed among these studies ($I^2 = 13.0\%$, $p = 0.323$; Fig. 1B). The combined results showed that high NUSAP1 expression was significantly relative to poor OS in various cancers (pooled HR = 2.09, 95%CI 1.72–2.54, $p < 0.001$; Fig. 1B). We conducted the sensitivity analysis via removing one study every time, found that the pooled HR for OS was not remarkably affected, indicating our results were reliable (Fig. 1C). No significant publication bias was observed via using Begg's funnel plot in HRs for OS ($P = 0.133$; Fig. 1D). Then stratified analyses were performed based on OS analysis type (multivariate or non- multivariate), cancer type (digestive system or others), sample size (> 100 or ≤ 100), and follow-up time (> 5 years or ≤ 5 years). The results suggested that high NUSAP1 expression predicted worse OS in all subgroups above (Supplementary Table 7 and Supplementary Fig. 2A-D). Significant heterogeneity was observed across researches in the subgroup of follow-up time with more than 5 years, indicating it was the source of heterogeneity. Additionally, Kaplan-Meier curves with log-rank analysis using data of TCGA database were applied to evaluate the influence of NUSAP1 expression on OS of above-mentioned cancer patients. In line with the results of our meta-analysis, we discovered that elevated NUSAP1 expression predicted poor OS in 10 types of solid cancers ($p < 0.001$, Fig. 1E). In addition, our meta-analysis through a fixed-effects model ($I^2 = 0\%$, $p = 0.802$) also revealed that high NUSAP1 expression predicted worse DFS (pooled HR = 2.39, 95%CI 1.63–3.49, $p < 0.001$) (Supplementary Fig. 3A). The sensitivity analysis indicated that the result was reliable and no publication bias for DFS was observed via Begg's funnel plot (Supplementary Fig. 3B and C).

As indicated in Supplementary Table 8, meta-analysis was performed to expound the correlation of NUSAP1 expression with clinicopathological parameters. Significant associations were observed between high NUSAP1 expression and more advanced TNM stage (OR = 3.96, 95%CI 2.27-6.90), lymph node metastasis (OR = 2.16, 95%CI 1.31-3.56), distant metastasis (OR = 13.54, 95%CI 3.19-57.49),
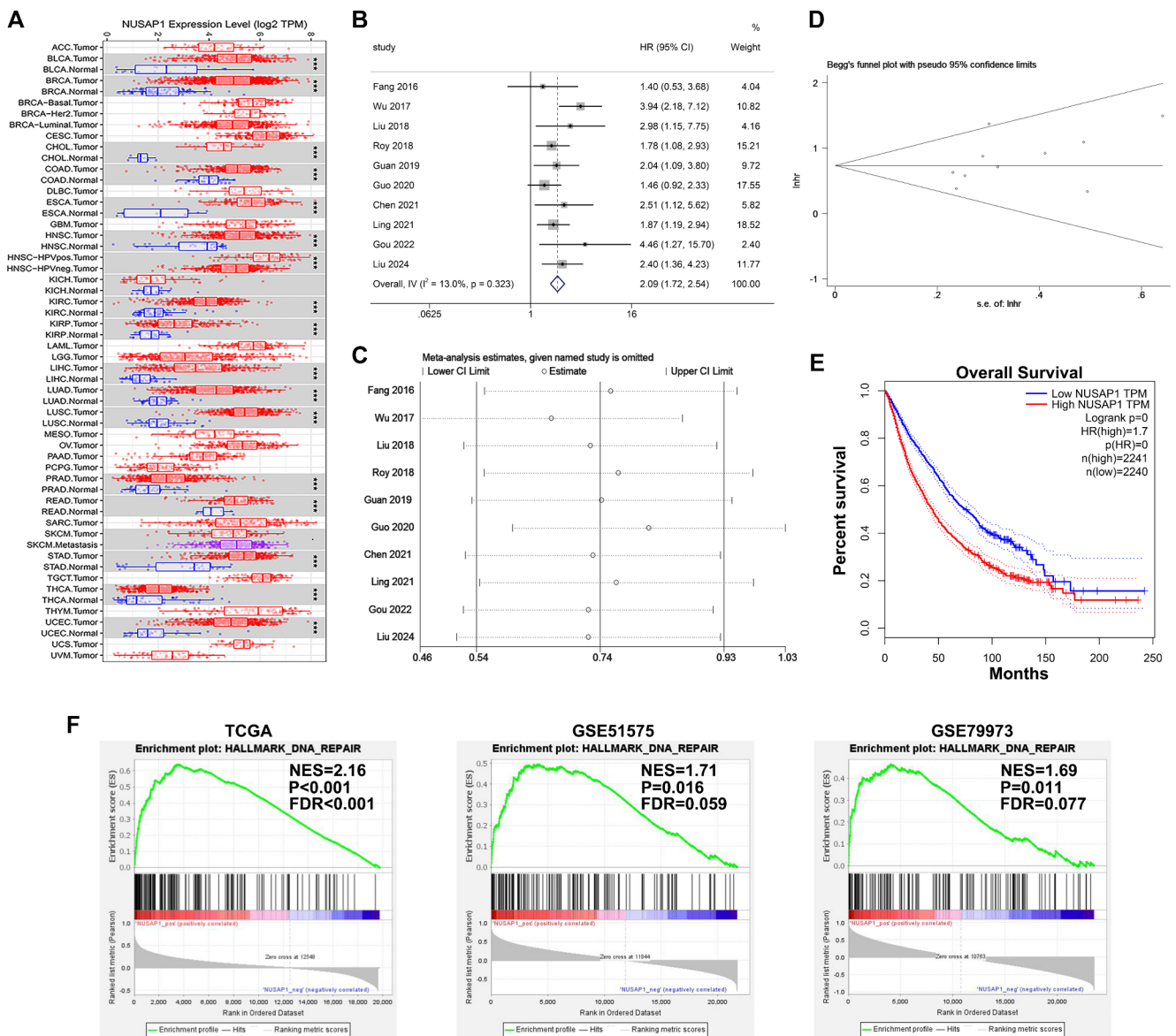
Fig. 1 Meta-analysis of the association of NUSAP1 expression with cancer prognosis and its GESA in GC. (**A**) The TIMER database analysis of NUSAP1 expression in all tumors, including GC. (**B**) Forest plot for the correlation between NUSAP1 expression and OS of cancer patients. (**C**) Sensitivity analysis of the included studies for OS. (**D**) Begg's funnel plots of the included studies for OS. (**E**) OS curves of NUSAP1 were plotted for various cancers from TCGA database using the GEPIA tool, including Kidney renal clear cell carcinoma (KIRC), Kidney renal papillary cell carcinoma (KIRP), Brain Lower Grade Glioma (LGG), Colon adenocarcinoma (COAD), Liver hepatocellular carcinoma (LIHC), Esophageal carcinoma (ESCA), Stomach adenocarcinoma (STAD), Bladder Urothelial Carcinoma (BLCA), Lung adenocarcinoma (LUAD), Lung squamous cell carcinoma (LUSC), Ovarian serous cystadenocarcinoma (OV), Pancreatic adenocarcinoma (PAAD). (n = 4481). (F) GSEA of NUSAP1 expression based on TCGA and GEO GC cohort. ***P < 0.001

low differentiation (OR = 2.76, 95%CI 1.18-6.48), but not for larger tumor size (Supplementary Fig. 4A-E).

Downregulation of NUSAP1 increased the radiosensitivity of GC cells

In our previous study, we found that NUSAP1 could promote proliferation, migration, and invasion of GC cells. Next, RNA sequencing data of TCGA and GEO (series: GSE51575 and GSE79973) databases were used to conduct GSEA. The results showed an obvious enrichment of the DNA repair-related signaling pathway in GC tissues with high NUSAP1 expression (Fig. 1F). It is well known that ionizing radiation can induce DNA double-strand breaks (DSB), radiosensitivity of tumor cells depends upon the ability of DNA damage repair(Sugase et al. 2017). It suggested that NUSAP1 may regulate the radiosensitivity of GC. Firstly, we measured NUSAP1 expression by western

blot in two GC cell lines after 4 Gy irradiation. As presented in Fig. 2A, the radiation induced upregulation of NUSAP1 in GC cells, which reached the peak at 48 h after irradiation. We knocked down NUSAP1 in the MKN-45 and HGC-27 cell lines via lentivirus-mediated infection. The transfection efficiency was examined by western blot (Supplementary Fig. 5A). Then the clonogenic survival assay was carried out to detect the influence of reducing NUSAP1 expression on GC cells radiosensitivity. As seen in Fig. 2B, NUSAP1 downregulation caused a substantial decrease of colony formation capacity in MKN-45 and HGC-27 cells after irradiation compared with the control group. The radiation survival curves contain parameters used to quantitively describe the effect, such as D_0 (the dose required to reduce survival to 37% of its value, namely mean lethal dose), Dq (the capability to accumulate sublethal damage), and SER (sensitization enhancement ratio). Lower D_0 or Dq indicates the elevated radiosensitivity. The D_0 values were 1.99 and 1.25 for NUSAP1 shRNA treated group in MKN-45 and HGC-27 cells, which were lower than the control groups (2.79 and 2.07, Fig. 2C). The SERs of MKN-45 and HGC-27 cells were 1.40 and 1.66, respectively.

Apoptosis is a vital mechanism of irradiation impairing tumor cells. We applied flow cytometry to elucidate the role of NUSAP1 on apoptosis induced by irradiation. The apoptosis rates in MKN-45 and HGC-27 cells with combination treatment of NUSAP1 knockdown and radiotherapy were remarkably increased when compared with those in cells treated by shNUSAP1 or irradiation alone (Fig. 2D). To further verify our results, we detected the apoptosis-related protein including p53, Bak, cleaved caspase 3, and Bcl-2. The pro-apoptotic proteins p53, Bak, and cleaved caspase 3 were significantly upregulated, while the anti-apoptotic protein Bcl-2 was obviously downregulated when combining irradiation and NUSAP1 knockdown, as compared with irradiation or silencing NUSAP1 alone (Fig. 2E). Taken together, NUSAP1 knockdown promoted the irradiation-induced apoptosis to reduce the radioresistance of GC cells.

NUSAP1 silencing attenuated DNA double-strand break repair in GC cells

Phosphorylation of H2AX on Ser139 (γH2AX) acted as a sensitive biomarker of DNA double-strand breaks. A strengthening in DNA damage manifested as the increased number of γH2AX focal points. To explore whether NUSAP1 could modulate IR-induced DSBs, we conducted immunofluorescence to calculate the number of γH2AX focal points at different time points after subjected to 4 Gy irradiation. Figure 3A and B showed that NUSAP1-deficient GC cells possessed more γH2AX foci per cell than the control group after 4 Gy irradiation. Then we performed

western bolt analyses of γH2AX expression and observed the similar results (Fig. 3C and D). In addition, the comet assay was adopted to detect DSB 24 h post-irradiation. The comet tails of GC cells transfected with shNUSAP1 were distinctly longer than the control group (Fig. 3E). These findings revealed that NUSAP1 downregulation suppressed the repair of IR-induced DSBs.

NUSAP1 downregulation improved the efficacy of irradiation in GC xenograft tumor models

We used nude mice bearing tumor xenografts to identify if NUSAP1 silencing increased the radiosensitivity of GC cells in vivo. Compared with the control group, the IR group and shNUSAP1 group presented the moderate reduction of tumor burden (IR: T/C%=46.56%; shNUSAP1: T/C = 57.22%) (Fig. 4A and B). Nevertheless, tumor growth suppression was more obvious when GC cells were treated by IR combined with shNUSAP1 (shNUSAP1 + IR: T/C = 14.38%) (Fig. 4C). We also observed an additive anti-tumor effect of the combined IR and shNUSAP1 by measuring the xenograft tumor weight (Fig. 4D). IHC analyses indicated that Ki-67 level was distinctly lower in tumors treated with IR in combination with shNUSAP1 than in those treated with either IR or shNUSAP1 alone (Fig. 4E).

## NUSAP1 protected ANXA2 against protein degradation via inhibiting its ubiquitination

To investigate the molecular mechanism underlying the influence of NUSAP1 on GC radiosensitivity, we conducted the immunoprecipitation assay to identify the NUSAP1-interacting proteins. Silver staining assay indicated that the NUSAP1 immunoprecipitated group exhibited several specific bands of proteins in comparison with the IgG group (Fig. 5A). According to the results of mass spectrometry, NUSAP1 bound with ANXA2 at a high binding score (Fig. 5B). Then we employed co-immunoprecipitation assays to confirm the physical binding between NUSAP1 and ANXA2. Western blot analyses determined that anti-NUSAP1 antibody could immunoprecipitate ANXA2 and that anti-ANXA2 could immunoprecipitate NUSAP1 (Fig. 5C). However, it was not clear if NUSAP1 influenced ANXA2 expression. Therefore, PCR assays were conducted to measure ANXA2 mRNA levels when NUSAP1 was silenced. We observed that there were no remarkable differences about the mRNA levels of ANXA2 between the shNUSAP1 and the control groups (Fig. 5D). Western blots indicated that ANXA2 protein levels were reduced when NUSAP1 expression was inhibited (Fig. 5E). Above results suggested that NUSAP1 could regulate the expression of ANXA2 at post-transcriptional level. The
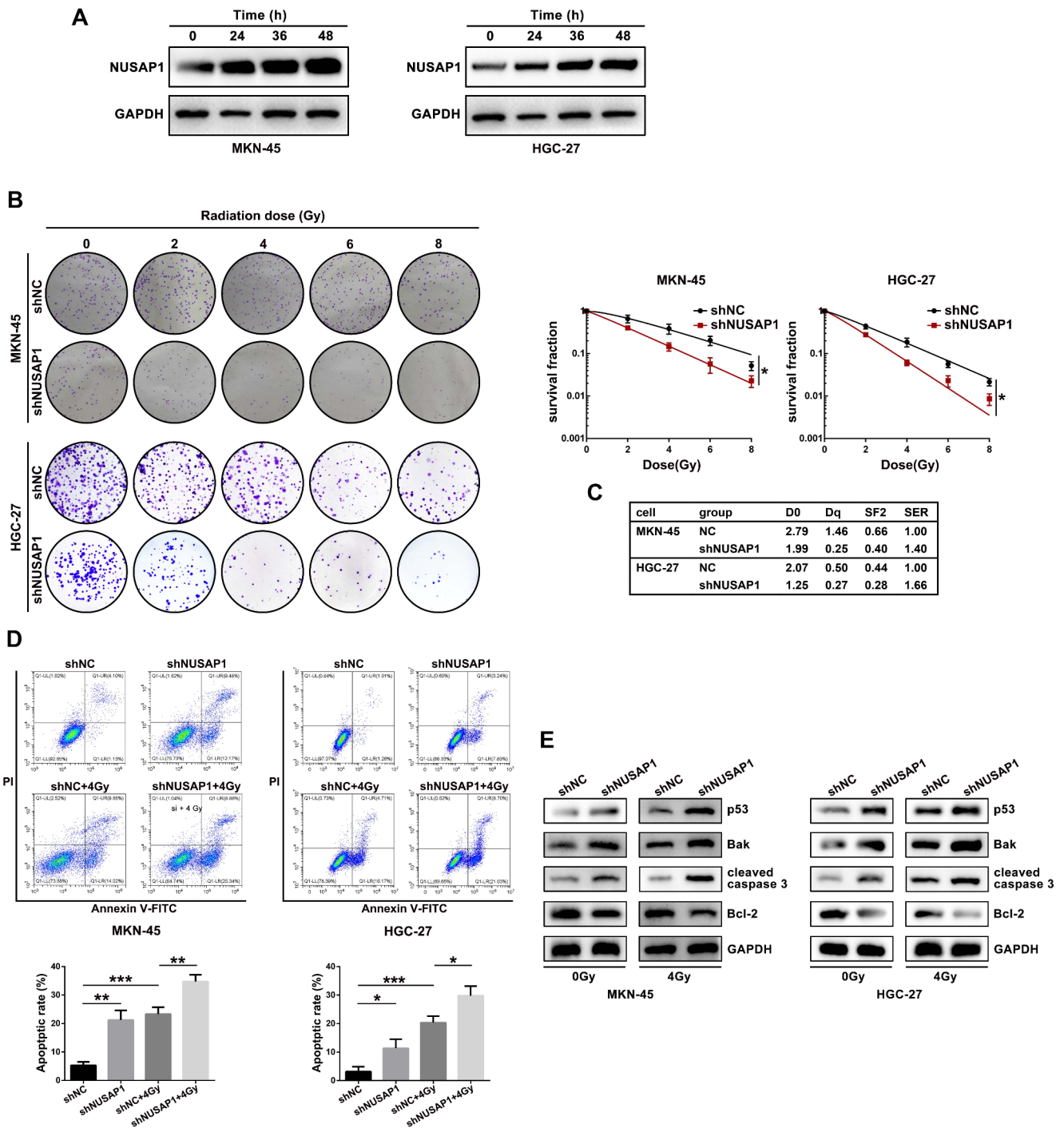
Fig. 2 Downregulation of NUSAP1 increased the radiosensitivity of GC cells. (**A**) Western blot was used to detected NUSAP1 expression at different time points after X-ray irradiation. (**B**) The colony formation assay and the irradiation dose-survival curves based on the single-hit multi-target model were utilized to measure the radiosensitivity of GC cells transfected with shNUSAP1 or negative control. (**C**) Radio-sensitivity parameters of respective cell groups. (**D**) Apoptosis rates of GC cells were detected by flow cytometry assay after 4 Gy X-ray irradiation. (**E**) Western blot analyses of apoptotic marker proteins in respective cell groups after irradiation exposure. Error bars indicated SD. *$P < 0.05$, **$P < 0.01$, ***$P < 0.001$
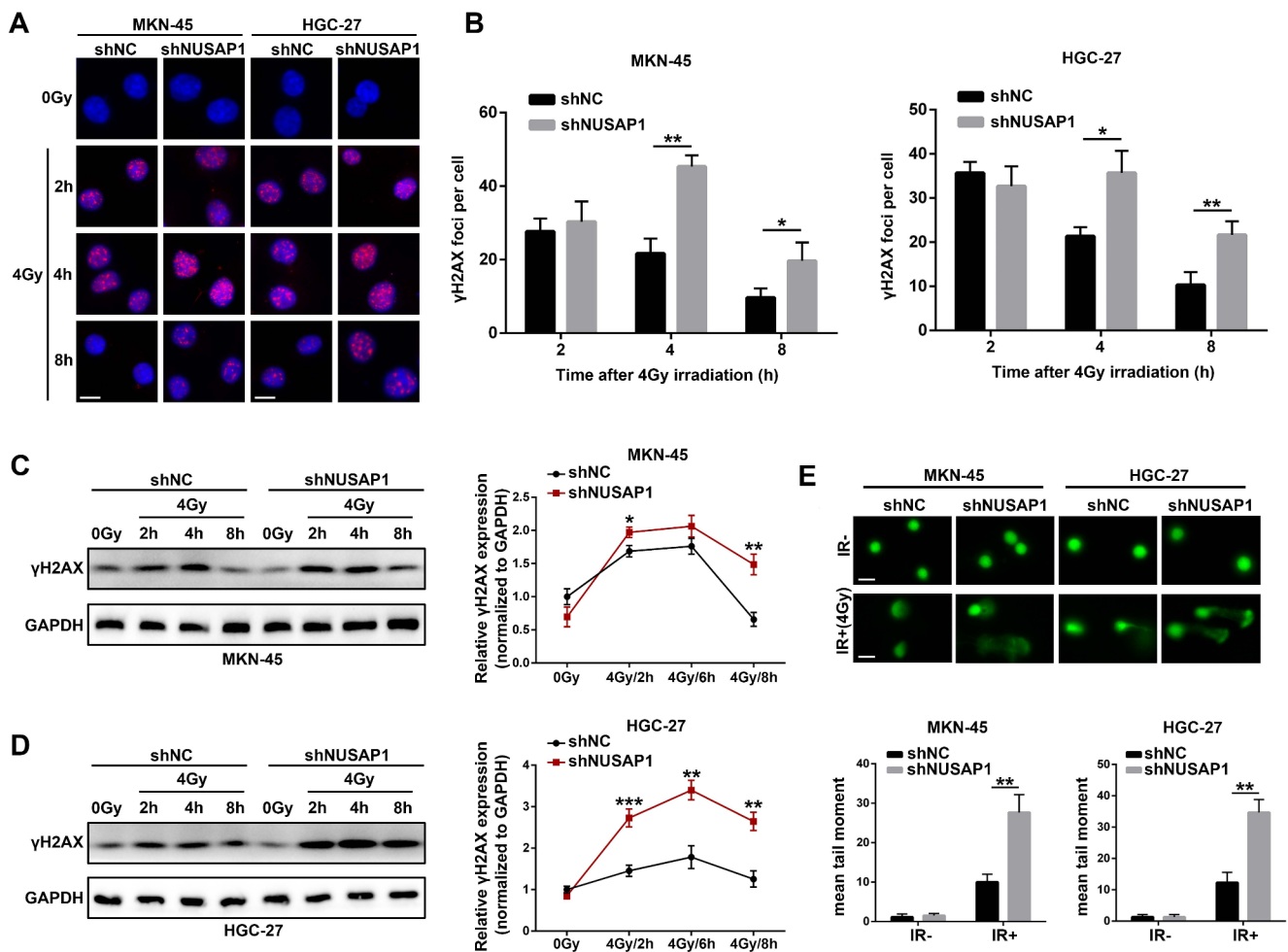
Fig. 3 NUSAP1 silencing attenuated DNA double-strand break repair in GC cells. (**A**, **B**) γ-H2AX foci in GC cells following NUSAP1 knockdown were evaluated by immunofluorescence staining after receiving 4 Gy irradiation. The foci number per cell was detected. Scale bar $= 10$ μm. (**C**, **D**) Western blot was performed to assess γ-H2AX expression in GC cells at different time points after irradiation exposure. (**E**) The comet assay was used to determine DNA double-strand break of GC cells in different treatment groups following 4 Gy of irradiation. Scale bar $= 25$ μm. Error bars indicated SD. $*P < 0.05$, $**P < 0.01$, $***P < 0.001$

ubiquitin–proteasome pathway is a common post-translational modification that is responsible for degrading 80–85% target proteins in eukaryotic organisms (Bustamante et al. 2018). It has been reported that ANXA2 protein levels could be changed by ubiquitination modification (Dai et al. 2023; Liu et al. 2023). NUSAP1 was previously found to stabilize ATR via antagonizing its ubiquitination (Zhao et al. 2020). We surmised NUSAP1 might also affected ANXA2 expression via the ubiquitin–proteasome pathway. To confirm this hypothesis, we evaluated the half-life of ANXA2 to explore whether NUSAP1 regulated AXNA2 protein stability through using CHX to treat the cell samples for different periods of time. Interestingly, NUSAP1 downregulation shortened the half-life of ANXA2 compared to that of the control group (Fig. 5F). Then we found that shNUSAP1-mediated degradation of ANXA2 was rescued by MG132, a protease inhibitor accurately inhibiting the ubiquitin–proteasome

pathway, which revealed that NUSAP1 was involved in regulating ANXA2 protein degradation via ubiquitination (Fig. 5G). As shown in Fig. 5H, the ubiquitination levels of ANXA2 were increased by NUSAP1 depletion. In a word, these results manifested that NUSAP1 enhanced the stability of ANXA2 through suppressing ubiquitination-mediated degradation.

NUSAP1 downregulation enhanced GC radiosensitivity through ANXA2

Firstly, the public databases were applied to predict the expression of ANXA2 in GC. RNA sequencing data from TCGA database using the GEPIA tool showed that ANXA2 was upregulated in GC tissues compared with normal tissues (Fig. 6A), which was similar to the expression pattern of ANXA2 observed in the GEO databases (series: GSE65801

A

MKN-45

B

C

D

E
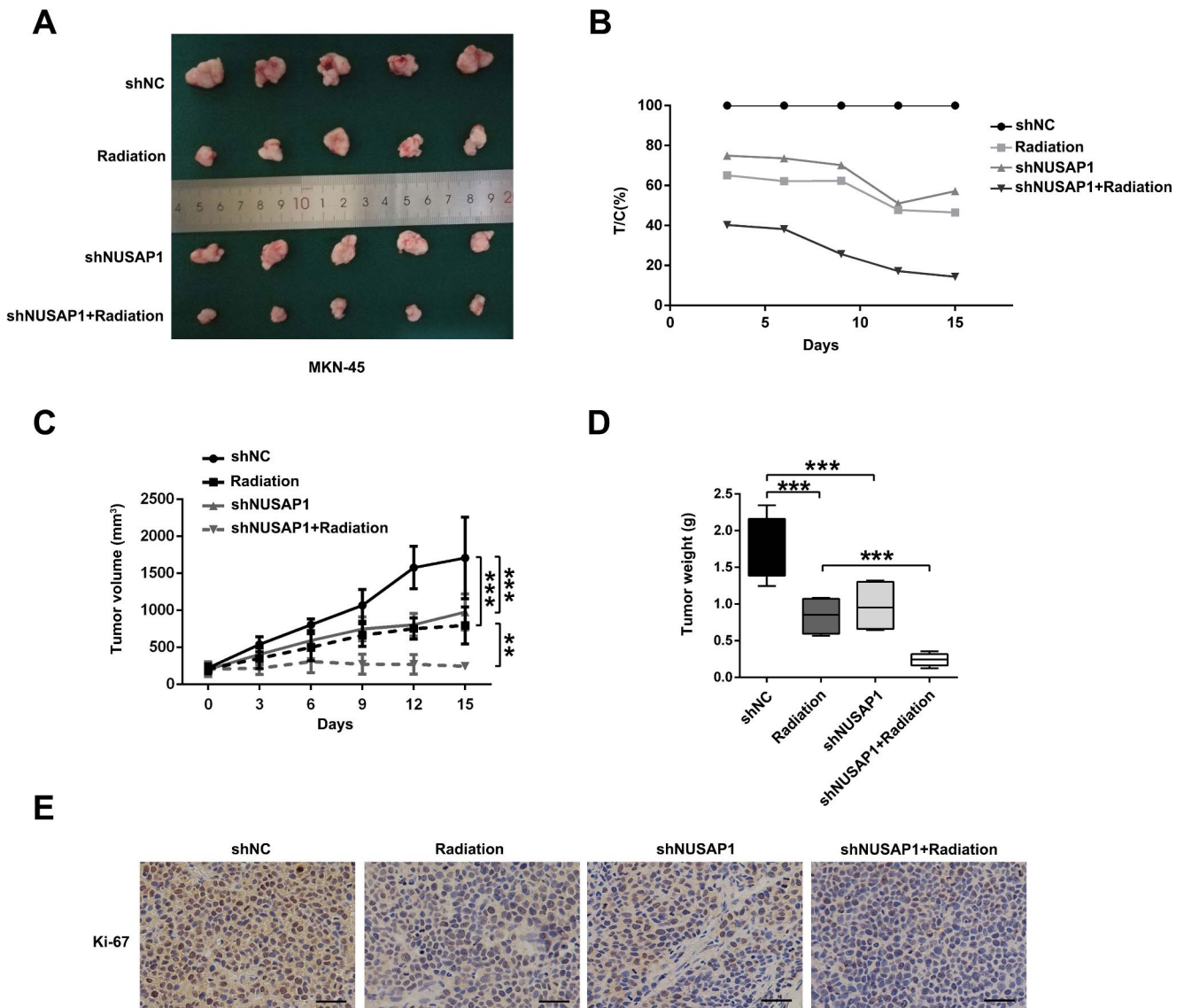
Fig. 4 NUSAP1 downregulation improved the efficacy of irradiation in GC xenograft tumor models. (**A**) Representative images of transplanted subcutaneous tumors from mice between various treatment groups and the negative control group. (**B**) Influence of NUSAP1 silencing and/or irradiation on the relative tumor proliferation rate of xenograft tumors in mice. (**C**) Tumor volumes of xenografts generated from the respective groups were calculated. (**D**) Tumor weight of xenografts in the respective groups was detected. (**E**) Representative images of Ki-67 in subcutaneous tumors of nude mice by IHC staining. Scale bar = 50 μm. Error bars indicated SD. **$*P < 0.01$, ***$P < 0.001$

and GSE51575) (Fig. 6B). Kaplan-Meier plots indicated that patients with high ANXA2 expression possessed poor overall survival and post progression survival (PPS) in GC (Fig. 6C and D). As previously reported, ANXA2 knockdown could increase radiosensitivity of nasopharyngeal carcinoma by activating the p38 MAPK-HSP27 pathway (He et al. 2022). Subsequently, we conducted GSEA based on TCGA database and discovered that ANXA2 expression was positively related with DNA repair-related signaling pathway in GC tissues (Fig. 6E), suggesting that ANXA2 might affect GC radiosensitivity. Then we adopted lentivirus-mediated infection to reduce ANXA2 expression and

confirmed the satisfactory transfection efficiency via western blot (Supplementary Fig. 5B). Following be subjected to increasing dose of irradiation, ANXA2-silenced GC cells showed decreased colony survival fractions (Fig. 6F and G). In addition, GC cells treated with shANXA2 existed higher expression of γH2AX at 8 h after receiving 4 Gy irradiation (Fig. 6H). Next, rescue experiments showed that overexpression of ANXA2 reversed the inhibitory effect on the colony formation capability of GC cells induced by shNUSAP1 following irradiation at various doses (Fig. 6I and J). Through these data, we concluded that knockdown of NUSAP1 increase GC radiosensitivity via ANXA2.
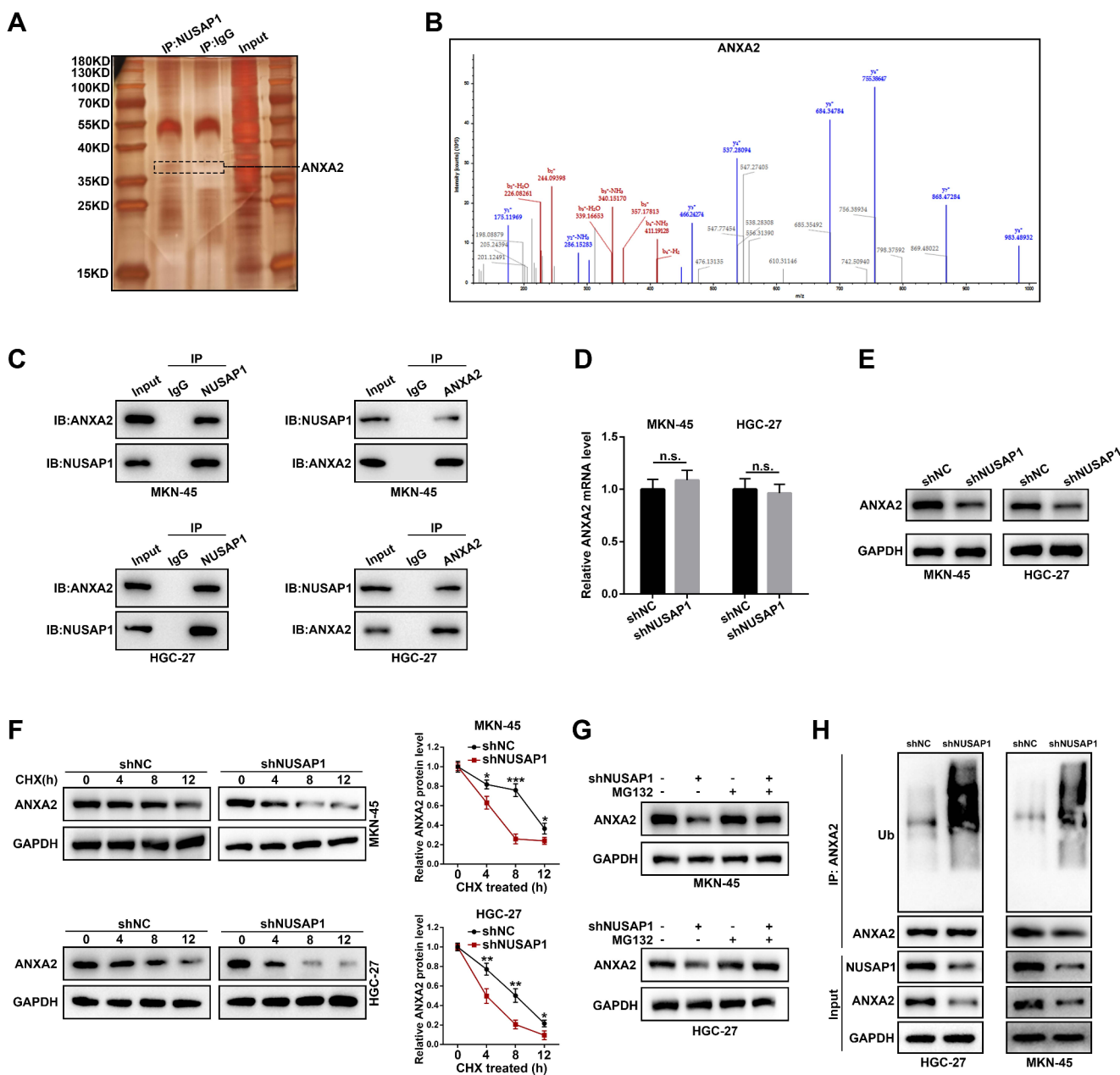
Fig. 5 NUSAP1 protected ANXA2 against protein degradation via inhibiting its ubiquitination. (**A**) Silver staining image of immunoprecipitation assay using anti-NUSAP1 antibody and IgG in HGC-27 cells. (**B**) Mass spectrometry image of ANXA2. (**C**) Extracts of GC cells were immunoprecipitated with anti-NUSAP1/anti-ANXA2 and control (IgG) antibodies. Co-immunoprecipitated proteins were detected through western blot with their respective antibodies. (**D**) qRT-PCR was conducted to evaluate the effects of NUSAP1 knockdown on ANXA2 mRNA levels. (**E**) Western blot was performed to measure the influence of NUSAP1 downregulation on ANXA2 pro-tein levels. (**F**) Half-life analysis of ANXA2 abundance in GC cells treated with shNUSAP1 or negative control for the indicated periods in the presence of CHX. Quantification of ANXA2 stability was exhibited on the right. (**G**) GC cells of different groups were treated with MG132 and ANXA2 protein levels were detected by western blot. (**H**) Immunoblotting analysis of the ubiquitination of ANXA2 in HGC-27 and MKN-45 cells transfected with NUSAP1 shRNA or corresponding control vector. Error bars indicated SD. *$P < 0.05$, **$P < 0.01$, ***$P < 0.001$

NUSAP1 was negatively regulated by miR-129-5p in GC

Aberrant NUSAP1 expression was likely regulated by miRNAs in GC. Starbase was used to predict the miRNAs

binding with NUSAP1. Combined with the following criterion (miRNA existed lower expression in TCGA GC tissues than normal tissues, $p < 0.05$), we screened out two miR-NAs (miR-129-5p and miR-193a-5p) (Fig. 7A). Firstly, we transfected miR-129-5p mimic, miR-193a-5p mimic, and
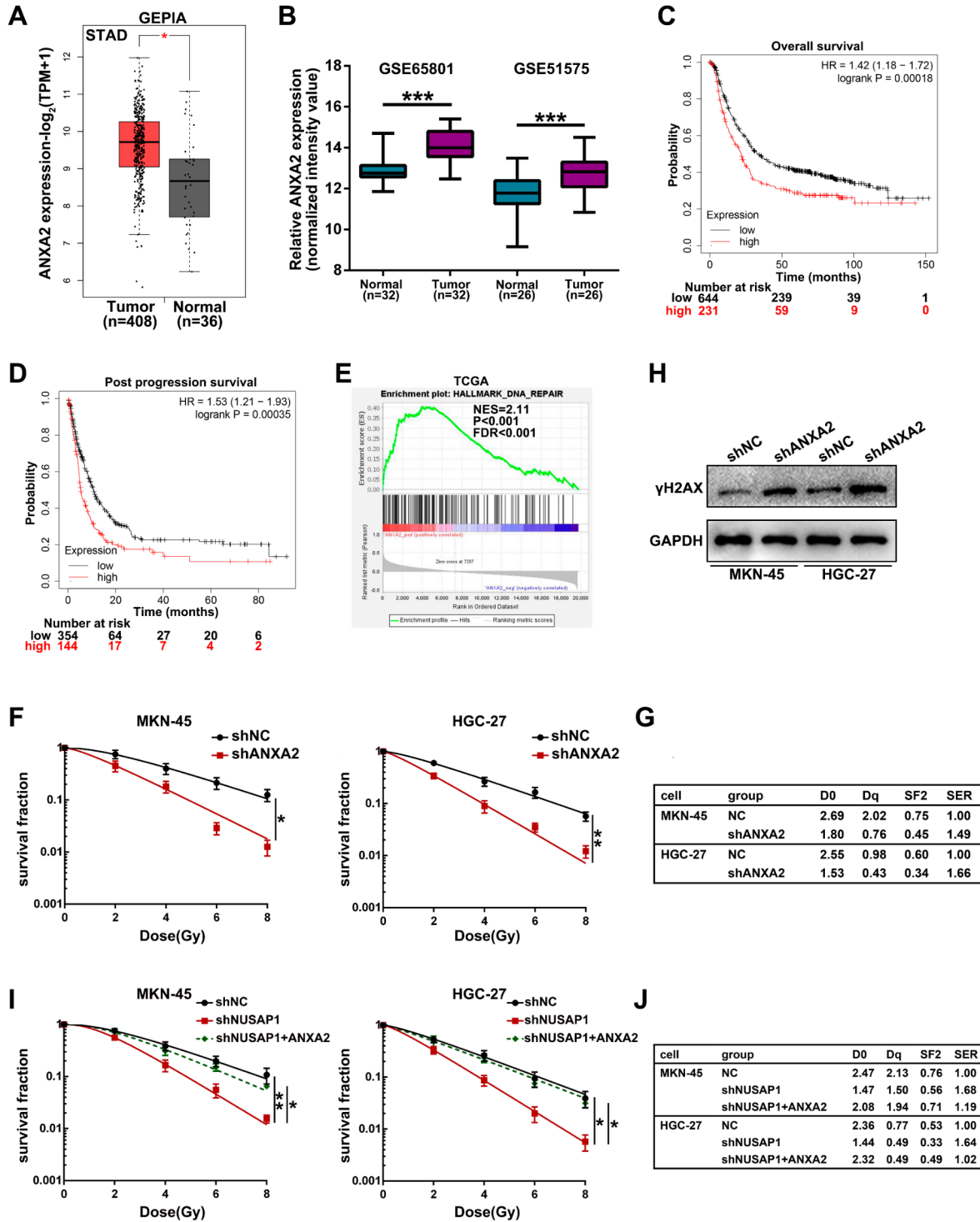
Fig. 6 NUSAP1 downregulation enhanced GC radiosensitivity through ANXA2. (**A**) Expression of ANXA2 in the TCGA GC cohort from GEPIA website. (**B**) ANXA2 expression in GC tissues was predicted by GEO database (series: GSE65801 and GSE51575). (**C**, **D**) Kaplan-Meier survival analyses of the OS (**C**) and PPS (**D**) of GC patients with high versus low ANXA2 expression in the TCGA cohort. The cutoff value is the median of NUSAP1 expression. (**E**) GSEA was performed to explore the signaling pathway impacted by ANXA2 based on TCGA GC cohort. (**F**, **G**) After ANXA2 was silenced, GC cells were treated to 2, 4, 6, or 8 Gy of X-ray radiation and the radiosensitivity of them was determined via the clonogenic survival assay. (**H**) γH2Ax expression in GC cells treated with ANXA2 shRNA or negative control was analyzed by western blot following exposed to 4 Gy irradiation. (**I**, **J**) Survival curves showing the effect of ANXA2 overexpression on shNUSAP1-induced radiosensitization. Error bars indicated SD. $*P < 0.05$, $**P < 0.01$, $***P < 0.001$
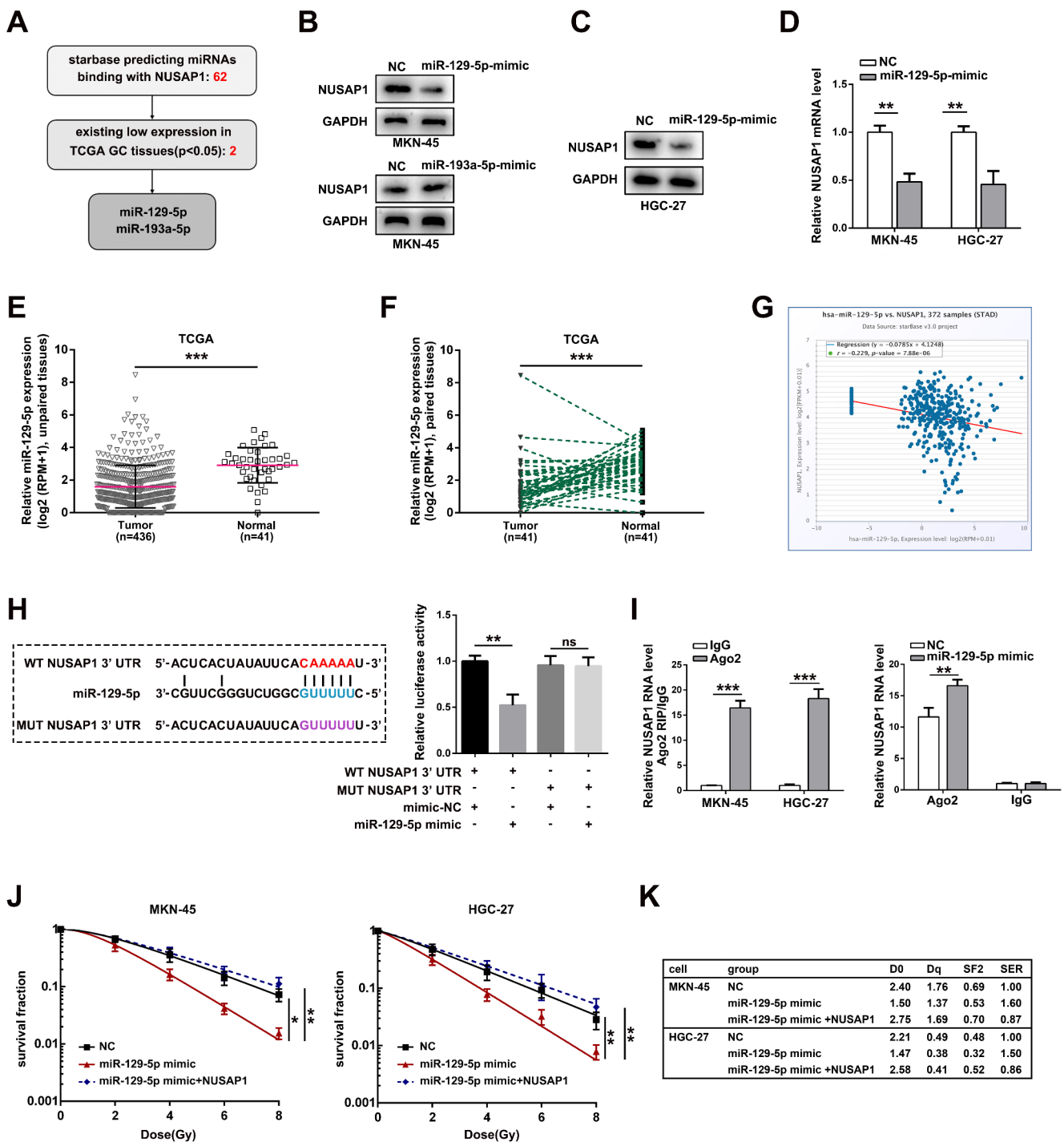
Fig. 7 NUSAP1 was negatively regulated by miR-129-5p in GC. (**A**) MiRNAs potentially binding with NUSAP1 were predicted by starbase, which simultaneously existed lower expression in TCGA GC tissues compared with normal tissues. (**B**) NUSAP1 protein levels were detected by western blot when MKN-45 cells were transfected with miR-129-5p mimic or miR-193a-5p mimic. (**C**) Western blot analysis of the protein level of NUSAP1 in HGC-27 cells treated by miR-129-5p mimic. (**D**) qRT-PCR analyses of NUSAP1 mRNA levels in GC cells treated by miR-129-5p mimic. (**E**, **F**) Data extracted from TCGA were used to evaluate the relative expression of miR-129-5p in unpaired and paired GC tissues. (**G**) The correlation of expression between NUSAP1 and miR-129-5p were assessed by starbase using TCGA GC cohort. (**H**) The predicted sequence alignment was shown, and the dual luciferase reporter assay was carried out to verify the binding between NUSAP1 and miR-129-5p. (**I**) Ago2-RIP experiments were conducted, and NUSAP1 RNA levels in the immunoprecipitants were detected by qRT-PCR assay. IgG was used as a negative control. (**J**) The radiosensitivity of respective groups (miR-129-5p mimic and miR-129-5p mimic + NUSAP1) was measured by the clonogenic survival assay. Error bars indicated SD. *$P<0.05$, **$P<0.01$, ***$P<0.001$

negative control into GC cells, respectively. QRT-PCR was used to verify the transfection efficiency (Supplementary Fig. 5C). Then western blot was conducted to determine the influence of above two miRNAs upregulation on NUSAP1 protein levels. As shown in Fig. 7B, NUSAP1 expression was significantly inhibited when overexpressing miR-129-5p instead of miR-193a-5p in MKN-45 cells, suggesting that NUSAP1 was the potential target gene of miR-129-5p. In HGC-27 cells, we also observed that miR-129-5p mimic caused the reduction of NUSAP1 protein level (Fig. 7C). Besides, the upregulation of miR-129-5p decreased the mRNA expression levels of NUASP1 in GC cells (Fig. 7D). Analyses of RNA sequence data from the TCGA database indicated that miR-129-5p expression was downregulated in GC tissues compared with unpaired or paired normal tissues (Fig. 7E and F). A negative association between miR-129-5p and NUSAP1 was presented in TCGA GC tissues (Fig. 7G). Next, we performed the dual-luciferase reporter assay to confirm the direct binding relationship and discovered that miR-129-5p mimic could dramatically reduce the luciferase activity of wild-type NUSAP1-3'UTR reporter other than mutant-type NUSAP1-3'UTR reporter (Fig. 7H). Ago2 is a key component of the RNA-induced silencing complex (RISC), playing a crucial role in miRNA-mediated target mRNA degradation. The Ago2-RIP experiment confirmed that NUSAP1 was specially enriched by Ago2 antibody than IgG antibody. Furthermore, miR-129-5p overexpression caused NUSAP1 preferentially accumulation in Ago2-containing beads in HGC-27 cells (Fig. 7I). The subsequent clonogenic survival assays indicated that GC cells treated with miR-129-5p mimic presented a remarkable increase in radiosensitivity (Fig. 7J and K). Rescue experiments were performed to explore whether NUSAP1 was a function target of miR-129-5p (Fig. 7J and K). The results showed that overexpression of NUSAP1 could reverse the enhancement of radiosensitivity mediated by miR-129-5p mimic.

Discussion

Gastric cancer possesses high morbidity and mortality rates globally. There are more than 420,000 new cases of GC in China every year, which accounts for nearly half of the world (Bray et al. 2018). The majority of GC patients in China are already in the advanced stage when they are diagnosed. In these subjects, using surgery is difficult to achieve a radical cure, while radiotherapy is important for the comprehensive treatment (Zhang et al. 2018). It is necessary to find the novel radiotherapeutic biomarkers for increasing the efficacy of radiotherapy in GC.

Our previous study illustrated that NUSAP1 expression was positively associated with tumor size and lymphatic metastasis in GC. Cell proliferation, migration, and invasion could be inhibited by NUSAP1 knockdown via suppressing mTORC1 signaling pathway (Ge et al. 2020). Recently, the accumulated evidence suggested NUSAP1 was abnormally expressed in various cancers and correlated with their poor survival as well as aggressive biological behaviors (Chen et al. 2023; Chiu et al. 2023; Liu et al. 2024). However, most researches assessing the prognostic value of NUSAP1 had the limitation of small sample size. So far, no comprehensive meta-analysis about the association of NUSAP1 expression with the prognosis of cancer patients was performed. In view of the critical role of NUSAP1 in cancer biology, we firstly conducted a meta-analysis and found that high expression of NUSAP1 predicted worse OS in ten types of solid cancers, which was also confirmed by the bioinformatics analysis. The subgroup meta-analyses also showed the similar results. In addition, our meta-analysis indicated that there was a close association between NUSAP1 high expression and more advanced TNM stage, lymph node metastasis, distant metastasis, and low differentiation. These results proved the vital clinical value of NUSAP1, likely acting as a biomarker of prognosis and clinical pathology in cancers.

GSEA indicated that high expression of NUSAP1 was positively associated with DNA repair-related signaling pathway. Several studies also have reported that NUSAP1 could regulate DNA damage repair in glioblastoma, chronic lymphocytic leukemia, prostate cancer, basal cell carcinoma, and hepatocellular carcinoma, in turn, influencing chemoresistance (Chiu et al. 2023; Han et al. 2021; Kong et al. 2023; Zhao et al. 2020; Zhu et al. 2023). The radiosensitivity of cancer cells depended on the ability of repairing irradiation-induced DNA damage (Qian et al. 2014). So, we speculated that NUSAP1 may be involved in the regulation of radiotherapy resistance in GC. We performed the relevant radiobiological experiments and observed that silencing NUSAP1 could suppress the colony formation capability, DNA repair ability, and increased the apoptotic percentage of GC cells after irradiation. Furthermore, through building a subcutaneous xenograft model, we identified that NUSAP1 downregulation enhanced the sensitivity of GC cells to radiation in vivo. Taken together, our results revealed that NUSAP1 could induce the radioresistance in GC.

To further explore the specific molecular mechanism of NUSAP1 in GC radioresistance, the immunoprecipitation and mass spectrometry were conducted. As a result, ANXA2 was found to bind with NUSAP1, and silencing NUSAP1 could decrease its protein expression level instead of its mRNA level, suggesting NUSAP1 regulated the expression of ANXA2 at post-transcriptional level. ANXA2 was a significant member of phospholipid binding protein family, which was originally reported to promote osteoclast formation and bone resorption (Menaa et

al. 1999). It was well established that elevated expression of ANXA2 was closely associated with various biological processes and poor prognosis in multiple cancers, including autophagy (Koh et al. 2024), angiogenesis (Shi et al. 2024), and mitochondrial homeostasis (Wang et al. 2023). Several researches reported that ANXA2 acted as a ubiquitination substrate. For instance, lncRNA HAR1A accelerated the interaction between TRIM65 and ANXA2, which induced ubiquitin-dependent degradation of ANXA2 in non-small cell lung cancer (Ling et al. 2024). FGF19 inhibited ANXA2 ubiquitination and subsequently promoted the malignant behaviors of nasopharyngeal carcinoma (Shi et al. 2024). Apart from the critical role in mitosis, Zhao et al. reported that NUSAP1 suppressed the ubiquitin-dependent proteolysis of ATR, potentiating chemoresistance in glioblastoma (Zhao et al. 2020). Our results also confirmed that using proteasome inhibitor MG132 rescued the reduction of ANXA2 protein levels caused by NUSAP1 downregulation, and NUSAP1 protected ANXA2 from ubiquitination. Our prediction by applying TCGA and GEO database identified a relatively increased ANXA2 expression in GC tissues. GC patients with high ANXA2 expression exhibited shorter overall survival and post progression survival. Similarly, GSEA showed that high expression of ANXA2 was enriched in DNA repair related signaling pathway. A previous study demonstrated that silencing ANXA2 increased the radiosensitivity via promoting G2/M-phase arrest, apoptosis, and activating the p38 MAPK-HSP27 pathway in nasopharyngeal carcinoma (He et al. 2022). However, no relevant research investigated the effects of ANXA2 on GC radiosensitivity. We obtained the same experimental result in GC that ANXA2 depletion suppressed colony formation and DSB repair efficacy of irradiated GC cells. Moreover, overexpressing ANXA2 could reverse NUSAP1 knockdown-induced the enhancement of radiosensitivity in GC cells. These results elucidated that NUSAP1 increased ANXA2 stabilization by inhibited its ubiquitination, conferring GC radioresistance.

Next, we investigated the upstream regulatory mechanism governing NUSAP1. MiRNAs are widely known for exerting biological effects by binding with the 3′UTR region of target mRNAs to regulate their expression (Lu and Rothenberg 2018). We identified NUSAP1 as the target of miR-129-5p based on starbase prediction, RIP, and luciferase reporter assays. Overexpressing miR-129-5p caused the reduction of NUSAP1 in mRNA and protein levels. Meanwhile, data from TCGA showed that miR-129-5p expression was downregulated and negatively correlated with NUSAP1 expression in GC tissues. MiR-129-5p has been recognized as a tumor suppressor, which decreased radioresistance in non-small cell lung cancer (Xue et al. 2021). Our results proved that miR-129-5p overexpression

dramatically increased the radiosensitivity of GC cells. Furthermore, NUSAP1 upregulation reversed the promoting effects on the radiosensitivity caused by miR-129-5p overexpression. Above findings suggested miR-129-5p increased GC radiosensitivity through the direct inhibition of NUSAP1 expression.

In conclusion, our study demonstrated that NUSAP1 high expression was associated with poor OS and DFS, as well as aggressive clinicopathologic features in human cancers via meta-analyses. We also confirmed that NUSAP1 induced radioresistance in GC. Mechanistically, we found that NUSAP1 could interact with ANXA2, which protected it from proteasomal degradation. NUSAP1 was suppressed by miR-129-5p. The results elucidated a novel axis miR-129-5p/NUSAP1/ANXA2 that participated in regulating GC radiosensitivity. NUSAP1 may be a potential target to overcome radioresistance of GC.

Data availability No datasets were generated or analysed during the current study.

Declarations

Ethical approval The animal experiments were reviewed and approved by the Ethics Committee of Nanjing Medical University (IACUC-2311002). Human tissue specimens were not involved in this study.

Competing interests The authors declare no competing interests.

References

Bray F, Ferlay J, Soerjomataram I, Siegel RL, Torre LA, Jemal A (2018) Global cancer statistics 2018: GLOBOCAN estimates of incidence and mortality worldwide for 36 cancers in 185 countries. CA Cancer J Clin 68(6):394–424. https://doi.org/10.3322/caac.21492

Bustamante HA, Gonzalez AE, Cerda-Troncoso C, Shaughnessy R, Otth C, Soza A, Burgos PV (2018) Interplay between the autophagy-lysosomal pathway and the ubiquitin-proteasome system: a target for Therapeutic Development in Alzheimer's Disease. Front Cell Neurosci 12:126. https://doi.org/10.3389/fncel.2018.00126

Chen L, Yang L, Qiao F, Hu X, Li S, Yao L, Shao ZM (2015) High levels of Nucleolar Spindle-Associated protein and reduced levels of BRCA1 expression Predict Poor Prognosis in Triple-negative breast Cancer. PLoS ONE 10(10):e0140572. https://doi.org/10.1371/journal.pone.0140572

Chen Y, Liu J, Zhang W, Kadier A, Wang R, Zhang H, Yao X (2021) O-GlcNAcylation enhances NUSAP1 Stability and promotes bladder Cancer aggressiveness. Onco Targets Ther 14:445–454. https://doi.org/10.2147/OTT.S258175

Chen M, Cen K, Song Y, Zhang X, Liou YC, Liu P, Liang T (2023) NUSAP1-LDHA-Glycolysis-lactate feedforward loop promotes Warburg effect and metastasis in pancreatic ductal adenocarcinoma. Cancer Lett 567:216285. https://doi.org/10.1016/j.canlet.2023.216285

Chiu CL, Li CG, Verschueren E, Wen RM, Zhang D, Gordon CA, Brooks JD (2023) NUSAP1 binds ILF2 to modulate R-Loop Accumulation and DNA damage in prostate Cancer. Int J Mol Sci 24(7). https://doi.org/10.3390/ijms24076258

Dai Y, Wei T, Huang Y, Bei Y, Lin H, Shen Z, Dai H (2023) Upregulation of HDAC9 in hippocampal neurons mediates depression-like behaviours by inhibiting ANXA2 degradation. Cell Mol Life Sci 80(10):289. https://doi.org/10.1007/s00018-023-04945-y

El-Hussieny M, Thabet DM, Tawfik HM, Gayyed MF, Toni ND (2024) The overexpression of NUSAP1 and GTSE1 could predict an unfavourable prognosis and shorter Disease Free Survival in ccRenal Cell Carcinoma. Asian Pac J Cancer Prev 25(7):2551–2559. https://doi.org/10.31557/APJCP.2024.25.7.2551

Fang L, Zhang M, Chen L, Xiong H, Ge Y, Lu W, Wu S (2016) Downregulation of nucleolar and spindle-associated protein 1 expression suppresses cell migration, proliferation and invasion in renal cell carcinoma. Oncol Rep 36(3):1506–1516. https://doi.org/10.3892/or.2016.4955

Ge Y, Li Q, Lin L, Jiang M, Shi L, Wang B, Xu Z (2020) Downregulation of NUSAP1 suppresses cell proliferation, migration, and invasion via inhibiting mTORC1 signalling pathway in gastric cancer. Cell Biochem Funct 38(1):28–37. https://doi.org/10.1002/cbf.3444

Gou R, Zheng M, Hu Y, Gao L, Wang S, Liu O, Lin B (2022) Identification and clinical validation of NUSAP1 as a novel prognostic biomarker in ovarian cancer. BMC Cancer 22(1):690. https://doi.org/10.1186/s12885-022-09753-4

Guan C, Liu Z, Lu C, Xiao M, Shi H, Ni R, Bian Z (2019) Nucleolar spindle-associated protein 1 promotes tumorigenesis and predicts poor prognosis in human esophageal squamous cell carcinoma. J Cell Biochem 120(7):11726–11737. https://doi.org/10.1002/jcb.28452

Guo H, Zou J, Zhou L, Zhong M, He Y, Huang S, Xiang X (2020) NUSAP1 promotes gastric Cancer Tumorigenesis and Progression by stabilizing the YAP1 protein. Front Oncol 10:591698. https://doi.org/10.3389/fonc.2020.591698

Han Y, Hu X, Yun X, Liu J, Yang J, Tian Z, Wang X (2021) Nucleolar and spindle associated protein 1 enhances chemoresistance through DNA damage repair pathway in chronic lymphocytic leukemia by binding with RAD51. Cell Death Dis 12(11):1083. https://doi.org/10.1038/s41419-021-04368-2

He H, Lin K, Zou C, Pan J, Fu W, Zhou Y, Su Y (2022) Knockdown of annexin A2 enhances radiosensitivity by increasing G2/M-Phase arrest, apoptosis and activating the p38 MAPK-HSP27 pathway in nasopharyngeal carcinoma. Front Oncol 12:769544. https://doi.org/10.3389/fonc.2022.769544

Koh M, Lim H, Jin H, Kim M, Hong Y, Hwang YK, Moon A (2024) ANXA2 (annexin A2) is crucial to ATG7-mediated autophagy, leading to tumor aggressiveness in triple-negative breast cancer cells. Autophagy 20(3):659–674. https://doi.org/10.1080/15548627.2024.2305063

Kong J, Xu S, Zhang P, Wang Y (2023) Transcription factor E2F8 promotes Cisplatin Resistance in Hepatocellular Carcinoma by regulating DNA damage via NUSAP1. Int J Toxicol 42(5):420–429. https://doi.org/10.1177/10915818231182114

Li C, Xue C, Yang Q, Low BC, Liou YC (2016) NuSAP governs chromosome oscillation by facilitating the kid-generated polar ejection force. Nat Commun 7:10597. https://doi.org/10.1038/ncomms10597

Li J, Tang M, Wu J, Qu H, Tu M, Pan Z, Hong J (2022) NUSAP1, a novel stemness-related protein, promotes early recurrence of hepatocellular carcinoma. Cancer Sci 113(12):4165–4180. https://doi.org/10.1111/cas.15585

Ling B, Wei P, Xiao J, Cen B, Wei H, Feng X, Huang W (2021) Nucleolar and spindle–associated protein 1 promotes non–small cell lung cancer progression and serves as an effector of myocyte enhancer factor 2D. Oncol Rep 45(3):1044–1058. https://doi.org/10.3892/or.2020.7918

Ling X, Qi C, Cao K, Lu M, Yang Y, Zhang J, Ma J (2024) METTL3-mediated deficiency of lncRNA HAR1A drives non-small cell lung cancer growth and metastasis by promoting ANXA2 stabilization. Cell Death Discov 10(1):203. https://doi.org/10.1038/s41420-024-01965-w

Liu Z, Guan C, Lu C, Liu Y, Ni R, Xiao M, Bian Z (2018) High NUSAP1 expression predicts poor prognosis in colon cancer. Pathol Res Pract 214(7):968–973. https://doi.org/10.1016/j.prp.2018.05.017

Liu ZY, Lin XT, Zhang YJ, Gu YP, Yu HQ, Fang L, Xie CM (2023) FBXW10-S6K1 promotes ANXA2 polyubiquitination and KRAS activation to drive hepatocellular carcinoma development in males. Cancer Lett 566:216257. https://doi.org/10.1016/j.canlet.2023.216257

Liu Y, Tang R, Meng QC, Shi S, Xu J, Yu XJ, Wang W (2024) NUSAP1 promotes pancreatic ductal adenocarcinoma progression by drives the epithelial-mesenchymal transition and reduces AMPK phosphorylation. BMC Cancer 24(1):87. https://doi.org/10.1186/s12885-024-11842-5

Lu TX, Rothenberg ME (2018) MicroRNA. J Allergy Clin Immunol 141(4):1202–1207. https://doi.org/10.1016/j.jaci.2017.08.034

Luo B, Feng S, Li T, Wang J, Qi Z, Zhao Y, Hu B (2022) Transcription factor HOXB2 upregulates NUSAP1 to promote the proliferation, invasion and migration of nephroblastoma cells via the PI3K/Akt signaling pathway. Mol Med Rep 25(6). https://doi.org/10.3892/mmr.2022.12721

Menaa C, Devlin RD, Reddy SV, Gazitt Y, Choi SJ, Roodman GD (1999) Annexin II increases osteoclast formation by stimulating the proliferation of osteoclast precursors in human marrow cultures. J Clin Invest 103(11):1605–1613. https://doi.org/10.1172/JCI6374

Park SH, Sohn TS, Lee J, Lim DH, Hong ME, Kim KM, Kang WK (2015) Phase III trial to compare Adjuvant Chemotherapy with Capecitabine and Cisplatin Versus Concurrent Chemoradiotherapy in Gastric Cancer: final report of the adjuvant chemoradiotherapy in stomach tumors trial, including survival and

subset analyses. J Clin Oncol 33(28):3130–3136. https://doi.org/10.1200/JCO.2014.58.3930

Qian D, Zhang B, Zeng XL, Le Blanc JM, Guo YH, Xue C, Yuan ZY (2014) Inhibition of human positive cofactor 4 radiosensitizes human esophageal squmaous cell carcinoma cells by suppressing XLF-mediated nonhomologous end joining. Cell Death Dis 5(10):e1461. https://doi.org/10.1038/cddis.2014.416

Qiu J, Xu L, Zeng X, Wu Z, Wang Y, Wang Y, Du Z (2021) NUSAP1 promotes the metastasis of breast cancer cells via the AMPK/PPARgamma signaling pathway. Ann Transl Med 9(22):1689. https://doi.org/10.21037/atm-21-5517

Raemaekers T, Ribbeck K, Beaudouin J, Annaert W, Van Camp M, Stockmans I, Carmeliet G (2003) NuSAP, a novel microtubule-associated protein involved in mitotic spindle organization. J Cell Biol 162(6):1017–1029. https://doi.org/10.1083/jcb.200302129

Roy S, Hooiveld GJ, Seehawer M, Caruso S, Heinzmann F, Schneider AT, Luedde T (2018) microRNA 193a-5p Regulates Levels of Nucleolar- and Spindle-Associated Protein 1 to Suppress Hepatocarcinogenesis. Gastroenterology, 155(6), 1951–1966 e1926. https://doi.org/10.1053/j.gastro.2018.08.032

Sexton RE, Hallak A, Diab MN, M., Azmi AS (2020) Gastric cancer: a comprehensive review of current and future treatment strategies. Cancer Metastasis Rev 39(4):1179–1203. https://doi.org/10.1007/s10555-020-09925-3

Shi S, Zhang Q, Zhang K, Chen W, Xie H, Pan S, You Y (2024) FGF19 promotes nasopharyngeal carcinoma progression by inducing angiogenesis via inhibiting TRIM21-mediated ANXA2 ubiquitination. Cell Oncol (Dordr) 47(1):283–301. https://doi.org/10.1007/s13402-023-00868-9

Smyth EC, Nilsson M, Grabsch HI, van Grieken NC, Lordick F (2020) Gastric cancer. Lancet 396(10251):635–648. https://doi.org/10.1016/S0140-6736(20)31288-5

Song Z, Wu Y, Yang J, Yang D, Fang X (2017) Progress in the treatment of advanced gastric cancer. Tumour Biol 39(7):1010428317714626. https://doi.org/10.1177/1010428317714626

Sugase T, Takahashi T, Serada S, Fujimoto M, Hiramatsu K, Ohkawara T, Naka T (2017) SOCS1 gene therapy improves radiosensitivity and enhances Irradiation-Induced DNA damage in esophageal squamous cell carcinoma. Cancer Res 77(24):6975–6986. https://doi.org/10.1158/0008-5472.CAN-17-1525

Tierney JF, Stewart LA, Ghersi D, Burdett S, Sydes MR (2007) Practical methods for incorporating summary time-to-event data into meta-analysis. Trials 8:16. https://doi.org/10.1186/1745-6215-8-16

Wang Y, Ju L, Xiao F, Liu H, Luo X, Chen L, Bian Z (2019) Downregulation of nucleolar and spindle-associated protein 1 expression suppresses liver cancer cell function. Exp Ther Med 17(4):2969–2978. https://doi.org/10.3892/etm.2019.7314

Wang Y, Wang Y, Liu W, Ding L, Zhang X, Wang B, Gao L (2023) TIM-4 orchestrates mitochondrial homeostasis to promote lung cancer progression via ANXA2/PI3K/AKT/OPA1 axis. Cell Death Dis 14(2):141. https://doi.org/10.1038/s41419-023-05678-3

Winkelmann RK, Black AK, Dover J, Greaves MW (1986) Pressure urticaria–histopathological study. Clin Exp Dermatol 11(2):139–147. https://doi.org/10.1111/j.1365-2230.1986.tb00438.x

Wu X, Xu B, Yang C, Wang W, Zhong D, Zhao Z, Zhang W (2017) Nucleolar and spindle associated protein 1 promotes the aggressiveness of astrocytoma by activating the hedgehog signaling pathway. J Exp Clin Cancer Res 36(1):127. https://doi.org/10.1186/s13046-017-0597-y

Xue T, Yin G, Yang W, Chen X, Liu C, Yang W, Zhu J (2021) MiR-129-5p promotes radio-sensitivity of NSCLC cells by targeting SOX4 and RUNX1. Curr Cancer Drug Targets 21(8):702–712. https://doi.org/10.2174/1568009621666210415094350

Yu JI, Lim DH, Lee J, Kang WK, Park SH, Park JO, Ahn S (2018) Necessity of adjuvant concurrent chemo-radiotherapy in D2-resected LN-positive gastric cancer. Radiother Oncol 129(2):306–312. https://doi.org/10.1016/j.radonc.2018.07.002

Zhang N, Fei Q, Gu J, Yin L, He X (2018) Progress of preoperative and postoperative radiotherapy in gastric cancer. World J Surg Oncol 16(1):187. https://doi.org/10.1186/s12957-018-1490-7

Zhang L, Dang Y, Wang Y, Fan X (2020) Nucleolar and spindle-associated protein 1 accelerates cellular proliferation and invasion in nasopharyngeal carcinoma by potentiating Wnt/beta-catenin signaling via modulation of GSK-3beta. J Bioenerg Biomembr 52(6):441–451. https://doi.org/10.1007/s10863-020-09860-6

Zhao Y, He J, Li Y, Lv S, Cui H (2020) NUSAP1 potentiates chemoresistance in glioblastoma through its SAP domain to stabilize ATR. Signal Transduct Target Ther 5(1):44. https://doi.org/10.1038/s41392-020-0137-7

Zhu Y, Liu Y, Zhang L, Zeng S, Xu W (2023) NUSAP1 regulates basal cell carcinoma migration, invasion and DNA damage through activation of the hedgehog signaling pathway. Physiol Int 110(2):160–172. https://doi.org/10.1556/2060.2023.00227